

# Combining Experimental and DFT Investigation of the Mechanism Involved in Thermal Etching of Titanium Nitride Using Alternate Exposures of NbF<sub>5</sub> and CCl<sub>4</sub>, or CCl<sub>4</sub> Only

Varun Sharma,\* Suresh Kondati Natarajan, Simon D. Elliott, Tom Blomberg, Suvi Haukka, Michael E. Givens, Marko Tuominen, and Mikko Ritala\*

Thermally activated chemical vapor-phase etching of titanium nitride (TiN) is studied by utilizing either alternate exposures of niobium pentafluoride (NbF<sub>5</sub>) and carbon tetrachloride (CCl<sub>4</sub>) or by using CCl<sub>4</sub> alone. Nitrogen (N<sub>2</sub>) gas purge steps are carried out in between every reactant exposure. Titanium nitride is etched in a non-self-limiting way by NbF<sub>5</sub>–CCl<sub>4</sub> based binary chemistry or by CCl<sub>4</sub> at temperatures between 370 and 460 °C. Spectroscopic ellipsometry and a weight balance are used to calculate the etch per cycle. For the binary chemistry, an etch per cycle of  $\approx 0.8$  Å is obtained for 0.5 and 3 s long exposures of NbF<sub>5</sub> and CCl<sub>4</sub>, respectively at 460 °C. On the contrary, under the same conditions, the etch process with CCl<sub>4</sub> alone gives an etch per cycle of about 0.5 Å. In the CCl<sub>4</sub>-only etch process, the thickness of TiN films removed at 460 °C varies linearly with the number of etch cycles. Furthermore, CCl<sub>4</sub> alone is able to etch TiN selectively over other materials such as Al<sub>2</sub>O<sub>3</sub>, SiO<sub>2</sub>, and Si<sub>3</sub>N<sub>4</sub>. X-ray photoelectron spectroscopy and bright field transmission electron microscopy are used for studying the post-etch surfaces. To understand possible reaction products and energetics, first-principles calculations are carried out with density functional theory. From thermochemical analysis of possible reaction models, it is found that NbF<sub>5</sub> alone cannot etch TiN while CCl<sub>4</sub> alone can etch it at high temperatures. The predicted byproducts of the reaction between the CCl<sub>4</sub> gas molecules and TiN surface are TiCl<sub>3</sub> and ClCN. Similarly, TiF<sub>4</sub>, NbFCl<sub>3</sub>, and ClCN are predicted to be the likely products when TiN is exposed to both NbF<sub>5</sub> and CCl<sub>4</sub>. A more favorable etch reaction is predicted when TiN is exposed to both NbF<sub>5</sub> and CCl<sub>4</sub> ( $\Delta G = -2.7$  eV at 640 K) as compared to exposure to CCl<sub>4</sub> only ( $\Delta G = -2$  eV at 640 K) process. This indicates that an enhanced etch rate is possible when TiN is exposed alternately to both NbF<sub>5</sub> and CCl<sub>4</sub>, which is in close agreement with the experimental results.

## 1. Introduction

With the continuous scaling of device dimensions in integrated circuits, more complex 3D device architectures are constantly being developed.<sup>[1,2]</sup> In order to keep developing such non-line-of-sight features, processing techniques that provide conformal as well as precise control of thickness at the atomic scale have become indispensable.<sup>[3–5]</sup> Deposition and etching are two of the most widely employed techniques in the fabrication of today's nanoelectronic devices. Semiconductor tool manufacturers have stretched their limits to gain atomic precision when depositing and etching various materials.<sup>[3–7]</sup> Atomic layer deposition is a well established chemical gas phase deposition technique with hundreds of reported processes.<sup>[8,9]</sup> On the other hand, reports on plasma-free chemical-based etch processes are limited and especially so for the recently developed thermal atomic layer etching (ALE).<sup>[10,11]</sup> Thermal ALE is a technique that uses sequential self-limiting surface-gas reactions in order to etch material from the surface.<sup>[12]</sup> The self-limiting surface reactions may provide important advantages, such as isotropic etching,<sup>[11,12]</sup> thickness control in the atomic regime and possibly improved etch selectivity. Therefore, thermal ALE is


V. Sharma, S. Haukka, M. E. Givens, M. Tuominen  
ASM Microchemistry Oy  
Pietari Kalmin katu 3 F2, Helsinki, Uusimaa 00560, Finland  
E-mail: varun.sharma@asm.com, varun.sharma@helsinki.fi

V. Sharma, M. Ritala  
Department of Chemistry  
University of Helsinki  
Helsinki, Uusimaa 00014, Finland  
E-mail: mikko.ritala@helsinki.fi

S. Kondati Natarajan  
Department of Electrical Engineering and Automation  
Aalto University  
Espoo 02156, Finland

S. D. Elliott  
Schrödinger  
120 West 45th Street, New York, NY 10036-4041, USA

T. Blomberg  
Department of Chemistry and Materials Science  
Aalto University  
Espoo, Uusimaa 02150, Finland

 The ORCID identification number(s) for the author(s) of this article can be found under <https://doi.org/10.1002/admi.202101085>.

DOI: 10.1002/admi.202101085

a promising technique for fabricating non-line-of-sight features in 3D nanoscale devices.

Titanium nitride (TiN) is a crucial material for the semiconductor industry due to its CMOS compatibility and has found use in applications such as tunable work-function metal gate<sup>[13]</sup> in FIN-field-effect-transistor and gate-all-around nanowire metal-oxide-semiconductor-field-effect-transistor,<sup>[14]</sup> gate electrode in metal-insulator-semiconductor field effect transistor,<sup>[15]</sup> diffusion barrier,<sup>[16]</sup> metal hard mask,<sup>[17]</sup> anti-reflective coating,<sup>[18]</sup> extreme ultra-violet patterning,<sup>[19]</sup> sub-bandgap<sup>[20]</sup> and Schottky photodetector,<sup>[21]</sup> and in plasmonics.<sup>[22,23]</sup>

So far, most of the TiN etch processes utilize either solutions<sup>[24–26]</sup> or plasma chemistries,<sup>[27–30]</sup> and a very few purely vapor etch processes have been reported.<sup>[31,32]</sup> Lee et al.<sup>[31]</sup> proposed a conversion-etch mechanism for TiN. First, the surface of the TiN films was oxidized to TiO<sub>2</sub> by ozone (O<sub>3</sub>) and then TiO<sub>2</sub> was etched by HF vapor in the form of volatile TiF<sub>4</sub> and H<sub>2</sub>O species. Ozone is a strong oxidant<sup>[31]</sup> and is capable of oxidizing also other materials in the vicinity on the integrated circuit chips. HF is toxic and its use may result in the dreaded fluorine contamination that not only affects the performance of CMOS devices but also poses compatibility issues with storage as well as semiconductor processing equipment. Thus, new thermal processes with other etchants for TiN would be beneficial in fabricating complex devices.

We report novel chemical etching processes for titanium nitride. Two types of etching processes were studied: first, a two-step gas-surface reaction based on sequential exposures of NbF<sub>5</sub>–CCl<sub>4</sub> reactants, and second a spontaneous etching by CCl<sub>4</sub> alone which can be defined as gas-phase pulsed etching (GPPE).<sup>[32]</sup> N<sub>2</sub> purge steps were introduced in between reactant pulses to avoid any reactant overlap, and to purge the etch system from excess reactant molecules as well as reaction products.

First principles calculations using density functional theory (DFT) are employed to study the thermochemistry of the reactions involved in the etch process. First principles calculations provide an effective approach for evaluating the free energies of the etch reactions. This is particularly important in this study as many exotic chemical species may be involved in the reaction for which experimental thermodynamic data are not available in the literature. We also use DFT to predict probable etch products from the product pressures evaluated at thermodynamic equilibrium.

## 2. Experimental Section

### 2.1. Substrates and Process Gases

P-doped silicon wafers of 200 mm diameter were chosen as substrates. The target films subjected to etching were SiO<sub>2</sub>, Si<sub>3</sub>N<sub>4</sub>, Al<sub>2</sub>O<sub>3</sub>, and TiN. The SiO<sub>2</sub> was either thermally grown silicon oxide of about 22 nm thick or 15 nm SiO<sub>2</sub> grown by the plasma-enhanced atomic layer deposition technique.<sup>[33]</sup> A 20 nm thick LPCVD nitride (Si<sub>3</sub>N<sub>4</sub>) was used. Al<sub>2</sub>O<sub>3</sub> of about 20 nm was deposited at 300 °C by the trimethylaluminum and water (H<sub>2</sub>O) ALD process.<sup>[34]</sup> TiN was deposited on 22 nm thermal oxide at 400 °C by thermal ALD process utilizing TiCl<sub>4</sub> and NH<sub>3</sub>.<sup>[35]</sup> The TiN films used in these etch experiments were from 10 to 50 nm in thickness.

NbF<sub>5</sub> (98%, CAS Number 7783-68-8) and anhydrous CCl<sub>4</sub> (CAS Number 56-23-5) were purchased from Sigma Aldrich, Inc. (Germany). The NbF<sub>5</sub> vessel was kept at 45–50 °C. The CCl<sub>4</sub> vessel was kept at room temperature and the vapors were drawn into the chamber. The CCl<sub>4</sub> dose was controlled by a needle valve and the NbF<sub>5</sub> outlet line did not have the needle valve installed. Nitrogen of 5.0 purity was used as a carrier gas, and was further purified by a purifier to ≥6.0 level.

### 2.2. Experimental Setup and Methodology

The etch experiments were performed in a Pulsar 2000 (P2000) reaction chamber, manufactured by ASM. The etch temperature was varied from 370 to 460 °C under isothermal conditions. Due to the hardware limitation of this particular P2000 module, the 460 °C was the maximum obtainable temperature and therefore the choice of the range. This temperature range may require highly thermally stable reactants such as CCl<sub>4</sub><sup>[36]</sup> and NbF<sub>5</sub>.<sup>[37,38]</sup> More details of a setup and methodology can be found in earlier reports.<sup>[32,39]</sup>

The etch rate per cycle (EPC) was calculated from the removed thickness values. Before and after etching, the thickness values were determined by spectroscopic ellipsometry (SE) and weight measurements as described earlier.<sup>[32]</sup> In order to verify the etch process, in situ grown TiN films were also subjected to etching. No significant differences in EPC were found between air-oxidized and in situ grown TiN films. In some cases, an X-ray reflectometer was also used to confirm the thickness and extract density values of TiN films. For simplicity, EPC values reported here were extracted from the weight measurements except in Figure 4, where SE thickness values are reported.

### 2.3. Characterization Techniques and Equipment

The SAG 204 balance from Mettler Toledo with a resolution of about 0.1 mg was used for the weight measurements. The EPC and removed thickness values were extracted by using simple mass–density–volume relationship, as described in previous report.<sup>[32]</sup>

For thickness, optical constants and density measurements the SE 800 (from SENTECH) ellipsometer and X'pert PRO XRR (from Malvern Panalytical Ltd.) were used.

The surface composition as well as depth profiles were determined with the help of X-ray photoelectron spectroscopy (XPS). The XPS used here was a K-Alpha<sup>+</sup> from Thermo Scientific. The aluminum Kα (1486.6 eV/15 kV) X-ray source was used with a spot size of about 400 μm. In the XPS depth profile measurements, the argon ion energy was set to 1000 eV. For the survey scan, a total of 10 scans were performed with a pass energy of 200 eV, and an increment of 0.5 eV.

The transmission electron microscopy was executed by Evans Analytical Group, California. For the imaging the FEI Tecnai TF-20 FEG/TEM operated at 200 kV was used in the bright-field TEM mode. For the sample preparation, an in situ focused ion beam (FIB) lift-out technique on an FEI dual beam FIB/SEM was used. Prior to the ion milling, the samples were carbon coated followed by sputtering iridium on top. The thickness of the TEM lamella was about 100 nm.

### 3. Theory and Computational Setup

The Vienna Ab initio Simulation Package (VASP v5.3)<sup>[40,41]</sup> was used for the quantum chemical calculations reported in this manuscript. We have used spin-polarized DFT to describe the electronic structure of the system under study. The exchange-correlation interactions are approximated by the Perdew–Burke–Ernzerhof<sup>[42]</sup> generalized gradient corrected density functional. The valence electrons are expanded in a plane wave basis set with a 400 eV cutoff, whereas the core electrons are treated by projector augmented wave (PAW) potentials.<sup>[43]</sup> The PAW potentials have 13 valence electrons for Nb, 4 for Ti, 5 for N, and 7 each for F and Cl. The geometries are relaxed within 1 meV of energy and within 0.02 eV Å<sup>−1</sup> of magnitude of each force component.

The cubic phase of TiN (space group Fm  $\bar{3}$  m) is chosen for the DFT study. The bulk unit cell consists of 4 TiN units and its shape and volume are simultaneously relaxed with a higher energy cutoff of 550 eV. A Monkhorst–Pack k-point mesh of 6 × 6 × 6 is used to sample the first Brillouin zone. The minimum energies of the isolated molecules are computed by optimizing their geometries within a noncubic box of dimensions 15 Å × 16 Å × 15.5 Å. The computation setup for the surface reaction are given in Section S0, Supporting Information.

For the reaction free energy computation, the free energy of a system at a given temperature  $T$  is given by

$$G = E + H - TS \quad (1)$$

in which  $E$  is the electronic energy of the system,  $H$  is the enthalpy and  $S$  is the entropy. Enthalpy and entropy of gas phase species are obtained from the “freeh” tool in the TURBO-MOLE suite.<sup>[44]</sup> The enthalpy and entropy of bulk systems are obtained with the Phonopy code,<sup>[45]</sup> which uses the force constants obtained from a density functional perturbation theory calculation in VASP with an energy threshold of  $1.0 \times 10^{-8}$  eV for the self consistent field evaluation of the electronic energy. The reaction free energy is then computed as

$$\Delta G = \Delta E + \Delta H - T\Delta S + RT \ln(\prod P_{\text{products}}^{\text{np}} / \prod P_{\text{reactants}}^{\text{nr}}) \quad (2)$$

in which the  $\Delta$  symbol signifies difference between the product and reactant state contributions. The “np” and “nr” are the number of gas phase molecules in the product state and reactant state, respectively.  $P$  is pressure and  $R$  is the gas constant. We can also calculate product pressure  $P_p$  at an user defined temperature  $T$  that will bring  $\Delta G = 0$ . If at some temperature  $T$ ,  $\Delta G$  without the  $RT \ln(Q)$  term is positive, then  $P_p$  value must be lowered to bring the reaction to equilibrium and vice versa. A very low value of  $P_p$  indicates that the corresponding reaction byproducts are less likely at that temperature and vice versa. Please note that this analysis cannot be used to obtain the product pressure value in Equation (2).

## 4. Results and Discussion

### 4.1. Thermochemistry: Free Energies of Proposed Reactions

Let us start by discussing the thermochemistry of the overall etch cycle and the individual reactant pulses using DFT data. In

**Table 1.** A list of reactions and computed thermochemistry representing the overall etch process in which 1 solid TiN bulk unit is converted into gas phase products on reacting with 1 NbF<sub>5</sub> and 1 CCl<sub>4</sub> molecules. R2, R4, and R5 (shown in bold font) are redox reactions. All species other than TiN are in gas phase.  $P_p$  at  $\Delta G = 0$  is the product pressure at 740 K that will bring the reaction to equilibrium at a constant reactant pressure of 2.5 Torr. A low  $P_p$  value indicates the reaction products are unlikely and vice versa.

	Reactions	$\Delta G$ [eV]		$P_p$ [Torr] at $\Delta G = 0$ ; $T = 740$ K
		640 K	740 K	
R1:	1 TiN + 1 NbF <sub>5</sub> + 1 CCl <sub>4</sub> → 1 TiCl <sub>3</sub> + 1 NbNFCI + 1 CF <sub>4</sub>	2.8	2.5	7.3E−14
R2:	1 TiN + 1 NbF <sub>5</sub> + 1 CCl <sub>4</sub> → 1 TiCl <sub>4</sub> + 1 NbNF + 1 CF <sub>4</sub>	3.3	2.9	1.5E−15
R3:	1 TiN + 1 NbF <sub>5</sub> + 1 CCl <sub>4</sub> → 1 TiCl <sub>3</sub> + 1 NbClF <sub>4</sub> + 1 CNF	−1.2	−1.6	3.8E+00
R4:	1 TiN + 1 NbF <sub>5</sub> + 1 CCl <sub>4</sub> → 1 TiCl <sub>4</sub> + 1 NbF <sub>4</sub> + 1 CNF	−0.8	−1.2	1.4E−01
<b>R5:</b>	<b>1 TiN + 1 NbF<sub>5</sub> + 1 CCl<sub>4</sub> → 1 TiF<sub>4</sub> + 1 NbFCI<sub>3</sub> + 1 ClCN</b>	−2.7	−3.1	3.8E+05

**Table 1** we show the reaction free energies for a number of reactions postulated for the overall etch cycle considering a reactant pressure of 2.5 Torr and a product pressure of 0.01 Torr. Please note that the product pressure cannot be controlled in an etch reactor and it is typically much lower than the reactant pressure, so we choose a value of 0.01 Torr for our calculations.

In reactions R1–R5, we consider a unit of bulk TiN reacting simultaneously with 1 NbF<sub>5</sub> and 1 CCl<sub>4</sub> molecules to form different gas phase products. It is to be noted that Nb can take different oxidation states and thus there are very many possible combinations of volatile products. Since it is not practical to consider all of them, we have computed a small set of representative product combinations.

The reactions R2, R4, and R5 (with labels in bold font in Table 1) are redox reactions in which the Ti atoms are oxidized and Nb atoms are reduced. The production of gaseous products is often entropically favored and therefore the reaction free energies decrease as the temperature is increased to 740 K (467 °C), with R5 being the most favorable at  $\Delta G = -3.1$  eV. R3 and R4 become favorable at 740 K although not as favorable as R5. At 640 K (367 °C), the favorable reactions are R3, R4, R5, and R9. R1 and R2 are more unlikely compared to R3 and R4 not because of the Ti compound but because of the Nb and C compounds. From the reaction energies, Nb–N compounds are found to be less favorable in gas phase when compared to C–N compounds. For a similar reason, R3 and R4 are more favorable than R1 and R2, respectively, although both reactions in each set form the same Ti compound. R5 is the most favorable, because it results in a C–N compound and TiF<sub>4</sub>, which is a well-known volatile and stable gas molecule. The TiF<sub>3</sub> as a byproduct was not considered due to its high boiling point of 1400 °C<sup>[31]</sup> and nonvolatility,<sup>[31,46]</sup> especially within the experimented temperature range, that is, 370–460 °C.

Even at 740 K, the calculations show that reactions R1 and R2 are not favorable as the change in Gibbs free energy is +2.5 and +2.9 eV, respectively. The product pressure evaluated at  $\Delta G = 0$  and 740 K gives an indication of the likelihood of the formation of the considered reaction products. This value is very small for

**Table 2.** Potential reactions of individual reagent pulses with bulk TiN in the etch process, assessed via thermochemistry computed with DFT. R6–R8 represent the fluorination pulse and R9 represents the chlorination pulse.  $P_p$  at  $\Delta G = 0$  is the product pressure at 740 K that will bring the reaction to equilibrium at a constant reactant pressure of 2.5 Torr. A low  $P_p$  value indicates the reaction products are unlikely and vice versa.

Reactions	$\Delta G$ [eV]		$P_p$ [Torr] at $\Delta G = 0$ ; T = 740 K
	640 K	740 K	
R6: $1 \text{ TiN} + 1 \text{ NbF}_5 \rightarrow 1 \text{ TiNF} + 1 \text{ NbF}_4$	6.1	5.7	7.3E–24
R7: $1 \text{ TiN} + 1 \text{ NbF}_5 \rightarrow 1 \text{ TiF}_3 + 1 \text{ NbNF}_2$	3.5	3.1	4.2E–15
R8: $1 \text{ TiN} + 1 \text{ NbF}_5 \rightarrow 1 \text{ TiF}_4 + 1 \text{ NbNF}$	3.9	3.5	2.5E–16
R9: $1 \text{ TiN} + 1 \text{ CCl}_4 \rightarrow 1 \text{ TiCl}_3 + 1 \text{ ClCN}$	–2	–2.4	1.8E+04

R1 and R2 suggesting that NbNF/Cl and  $\text{CF}_4$  are not very probable products. On the other hand, a high product pressure at  $\Delta G = 0$  and 740 K is registered for reaction R5 indicating an increased likelihood in the formation of the volatile products  $\text{TiF}_4$ ,  $\text{NbFCl}_3$ , and  $\text{ClCN}$ , hence the etching.

The reactions where  $\text{N}_2$  is an etch product were also considered, and are as follows:  $2 \text{ TiN(s)} + 6 \text{ NbF}_5(\text{g}) + 6 \text{ CCl}_4(\text{g}) \rightarrow 6 \text{ NbFCl}_3(\text{g}) + \text{N}_2(\text{g}) + 2 \text{ TiCl}_3(\text{g}) + 6 \text{ CF}_4(\text{g})$ , and  $2 \text{ TiN(s)} + 8 \text{ NbF}_5(\text{g}) + 8 \text{ CCl}_4(\text{g}) \rightarrow 8 \text{ NbFCl}_3(\text{g}) + \text{N}_2(\text{g}) + 2 \text{ TiCl}_4(\text{g}) + 8 \text{ CF}_4(\text{g})$ . Both the reactions are highly endothermic and unfavorable even at 500 K with reaction energies of 9.5 and 8.5 eV, respectively.

In Table 2, we consider representative etch reactions (R6–R9) in the individual pulses when either  $\text{NbF}_5$  or  $\text{CCl}_4$  is used as reactant. The fluorination pulse is presented as reactions R6–R8, in which  $\text{NbF}_5$  may interact with TiN and form gas phase  $\text{TiF}_x$  and  $\text{NbNF}_y$  species. The reaction free energies are very high (+3.1 to +5.7 eV at 740 K). The product pressure at  $\Delta G = 0$  and 740 K is correspondingly very small. This indicates that etch reactions are not possible when pulsing only  $\text{NbF}_5$  mainly due to the unfavorable Nb–N compounds. The adsorption mechanism of  $\text{NbF}_5$  on the TiN surface has been computed and is described in Section S1, Supporting Information. We find that  $\text{NbF}_5$  dissociates on the TiN(211) surface spontaneously at 400 K and results in the formation of strong surface bound Ti–F and Nb–N bonds (see Section S1, Supporting Information). Thermodynamically, the Ti–F bonds on TiN surface are more stable and favorable when compared to Ti–Cl bonds (see Section S3, Supporting Information). The formation of any gas phase byproducts was not observed from the DFT simulations of the fluorination pulse.

Reaction R9 shows the TiN etch reaction by  $\text{CCl}_4$  and a spontaneous etching at 640 and 740 K, as evidenced by the negative free energy change, is observed. The preferred products are  $\text{TiCl}_3$  and  $\text{ClCN}$ . Expressed in another way, the product pressure at  $\Delta G = 0$  and 740 K is very large. From simulations, we also found that  $\text{CCl}_4$  molecule dissociated spontaneously on TiN(211) surface (see Section S2, Supporting Information).

Thus, the first principles thermochemistry suggests that the  $\text{NbF}_5$  pulse could not etch (TiN) by itself, while the  $\text{CCl}_4$  pulse alone could etch (TiN) spontaneously, however subject to kinetic barriers. Comparing R5 and R9, the combination of ( $\text{NbF}_5$ ) and ( $\text{CCl}_4$ ) pulses at 740 K is predicted to give more effective etching of TiN than etching by  $\text{CCl}_4$  alone. The C compound in the two reactions is the same  $\text{ClCN}$  and the Ti

compounds  $\text{TiCl}_3$  and  $\text{TiF}_4$  have very similar thermochemistry as well. However,  $\text{NbFCl}_3$  offers lower zero point energy and higher entropy than  $\text{NbF}_5$  which allowed R5 to have a lower reaction free energy than R9.

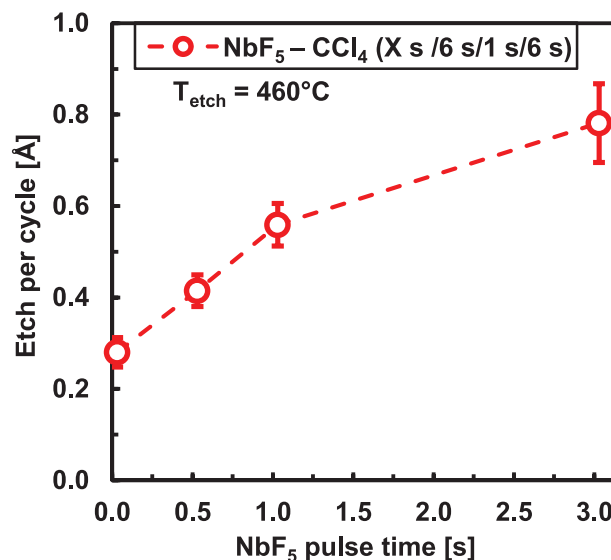
From simulations, a  $\text{CCl}_4$  is found to dissociate spontaneously at a surface bound fluorine free Nb site—which is the precursor for the formation of  $\text{NbF}_x\text{Cl}_y$  species in R9. Please refer to Section S2, Supporting Information of the Supporting Information for more information on the explicit reaction mechanisms that have been computed with DFT for this etch process. This enhanced etching phenomenon with sequential pulses of  $\text{NbF}_5$  and  $\text{CCl}_4$  is experimentally verified and observed in Figures 2 and 3.

## 4.2. Experimental Etching Characteristics

TiN films were etched by two types of etch processes: 1) a binary process that involves alternating exposures of  $\text{NbF}_5$  and  $\text{CCl}_4$  reactants in a cyclic manner and 2) a pulsing  $\text{CCl}_4$  alone in a chemical vapor etching (CVE) or GPPE process. One cycle of pulsed CVE of TiN films consists of a  $\text{CCl}_4$  exposure followed by an inert gas ( $\text{N}_2$ ) purge. The  $\text{N}_2$  purges were introduced to ensure the products and excess precursor molecules were removed properly from the etch system.

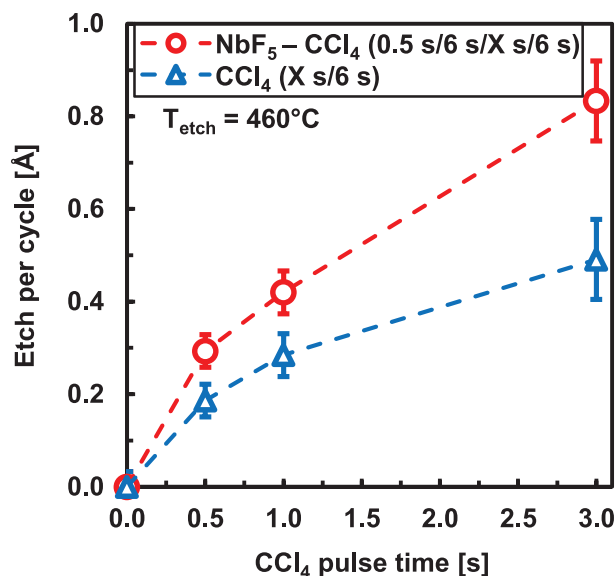
In this context, an etch system is an aggregate term used to describe all the components such as gas lines, valves and the reaction chamber and its parts. The concept and feasibility studies performed under this section demonstrate TiN etching in the atomic regime. The  $\text{CCl}_4$  based CVE process provides selectivity over  $\text{Al}_2\text{O}_3$ ,  $\text{SiO}_2$ , and  $\text{Si}_3\text{N}_4$ . However, the  $\text{NbF}_5$ – $\text{CCl}_4$  based etch process is able to etch  $\text{Al}_2\text{O}_3$  and provides selectivity over  $\text{SiO}_2$  and  $\text{Si}_3\text{N}_4$ .<sup>[39]</sup>

Figure 1 shows a change in the TiN EPC with varying  $\text{NbF}_5$  pulse time for the  $\text{NbF}_5$ – $\text{CCl}_4$  etch process at 460 °C and 1 s long  $\text{CCl}_4$  pulse time. The etch temperature of 460 °C was chosen



**Figure 1.** Etch per cycle for TiN films versus  $\text{NbF}_5$  pulse time at 460 °C. The duration of  $\text{N}_2$  purges and  $\text{CCl}_4$  pulses were fixed at 6 and 1 s, respectively.





**Figure 2.** Etch per cycle of TiN films with varying CCl<sub>4</sub> pulse time at 460 °C. 6 s long N<sub>2</sub> purges were used. The figure compares the EPC for the binary process (red) to the CVE process (blue).

because it was limited by the hardware. The figure reveals that when no NbF<sub>5</sub> is used, an EPC of 0.3 Å is obtained which indicates that CCl<sub>4</sub> alone is capable of etching TiN films as will be discussed later. This is consistent with the favorable thermochemistry that is predicted with DFT. The EPC increases from 0.3 to about 0.6 Å when the NbF<sub>5</sub> pulse time is varied from 0 to 1 s. At 3 s NbF<sub>5</sub> pulse time an EPC of about 0.8 Å is measured. There is no clear saturation of EPC with the NbF<sub>5</sub> pulse time, but a marginal slowing of an EPC is observed. We speculate that this nonsaturated behavior can be attributed to various factors such as partially self-limiting nature of the surface reaction, insufficient purge time, low volatility, or otherwise slow removal of the products from the TiN surface and presence of finite vapors of CCl<sub>4</sub> in the etch system. This soft-saturation of the EPC with NbF<sub>5</sub> pulse time can also be assigned to a slow diffusion of F species through grain boundaries to form a converted TiN surface and form fluorinated TiN surface.

In **Figure 2** EPCs for two etch processes are plotted against CCl<sub>4</sub> pulse time at an etch temperature of 460 °C. From the graph, it is worth noticing that the EPC for the NbF<sub>5</sub>-CCl<sub>4</sub> etch process is higher than that for the CCl<sub>4</sub> only CVE process. This holds true for a given set of process parameters such as gas flows, partial pressure of both the precursors, the pulse and purge times up to 3 and 6 s, respectively, and total pressure of the reaction chamber.

The earlier presented first principles simulations also predicted a more favorable etch reaction for the NbF<sub>5</sub>-CCl<sub>4</sub> process than for CCl<sub>4</sub> only. For both etch processes, the EPC tends to increase with the CCl<sub>4</sub> pulse time.

Figure 2 shows that no etching was observed when 0.5 s of NbF<sub>5</sub> and no CCl<sub>4</sub> was used, for total 300 cycles. No change in the TiN thickness was observed even after 300 cycles of 1 s NbF<sub>5</sub> pulse. At temperatures below 460 °C, NbF<sub>5</sub> alone was not able to etch TiN by itself. This is consistent with the first principles simulations. The TiN thickness values before and after NbF<sub>5</sub> exposure were confirmed by XRR measurements.

For both etch processes, no clear saturation of EPC is observed. The EPC continues to increase linearly with CCl<sub>4</sub> pulse time from 0.5–3.0 s, with no sign of saturation. At 3 s long CCl<sub>4</sub> pulse time, EPC values of about 0.8 and 0.5 Å are observed for the NbF<sub>5</sub>-CCl<sub>4</sub> and CCl<sub>4</sub> only CVE processes, respectively. NbF<sub>5</sub> enhances the etch rate of TiN and this could be due to an enhanced reactivity of the CCl<sub>4</sub> with fluorinated TiN surface or the formation of more volatile species such as TiCl<sub>4</sub> (R5 in Table 1) instead of TiCl<sub>3</sub>,<sup>[47]</sup> TiOCl, or TiF<sub>3</sub>. The TiCl<sub>3</sub> at 427 °C, has a sufficiently high vapor pressure of 37 mTorr.<sup>[48]</sup> On the contrary, TiF<sub>3</sub> has a very high boiling point of 1400 °C<sup>[31]</sup> and is nonvolatile.<sup>[31,46]</sup> The vapor pressures of TiCl<sub>4</sub> and TiF<sub>4</sub> at 90 °C are 190 Torr<sup>[49]</sup> and 18 mTorr,<sup>[50]</sup> respectively.

Another possible reason for the faster etching could be fluorine species diffusing through the TiN grain boundaries and therefore the etching may proceed three dimensionally rather than being limited to the surface. Later in Figure 7, the XPS depth profile analysis did show some fluorine penetration into the remaining TiN film, after exposing it to the NbF<sub>5</sub>-CCl<sub>4</sub> CVE process.

The simulation results provided in the Supporting Information (see Section S2, Supporting Information) reveal that the Nb sites are important for CCl<sub>4</sub> to react with when the rest of the surface is covered with F. It is found that the a favorable binding between the Cl atoms and Nb atom is possible (more details in the Section S2, Supporting Information) even when the Nb atom is weakly bound to 2 F atoms. However, a strong dissociative adsorption of CCl<sub>4</sub> (−3.2 eV) is possible when the Nb atom is free of Nb–F bonds (see Figure S5b, Supporting Information) in the Supporting Information). Based on the computational results, we propose that the ALE of TiN proceeds by self-limiting reaction of NbF<sub>5</sub> molecules with TiN surface in the first pulse (see Section S1, Supporting Information) followed by the dissociative adsorption of CCl<sub>4</sub> catalyzed by the Nb sites in the second pulse leading to the etch of TiN. Additionally, from the two it can be seen that the NbF<sub>5</sub> alone did not etch TiN and is predicted by the computational results.

In **Figure 3**, the effect of etch temperature on etch per cycle is captured for the both etch processes. The NbF<sub>5</sub> and CCl<sub>4</sub> pulse times were set to 1 s with 6 s long N<sub>2</sub> purges. For the data points in this graph, a total of 200, 200, 300, and 400 etch cycles were performed at etch temperatures of 370, 380, 400, and 460 °C, respectively. For the NbF<sub>5</sub>-CCl<sub>4</sub> etch process, a low EPC of 0.03 Å per cycle at 370 °C is obtained and the EPC increases almost linearly to about 0.4 Å per cycle at 400 °C. At 460 °C, a higher etch rate of 0.55 Å per cycle is noted. In contrast, the CCl<sub>4</sub> only etch process shows an etch rate of 0.07 Å per cycle at 370 °C and linearly increases to about 0.3 Å per cycle at 460 °C. Both the etch processes were unable to etch TiN significantly at temperatures below 370 °C, even after total 1000 etch cycles. This is in disagreement with DFT thermochemistry predictions, which shows possible etching at 500 K (227 °C) and the reason for this can be due to higher activation barrier.

### 4.3. Etch Selectivity

Etch selectivity of TiN against different materials such as Al<sub>2</sub>O<sub>3</sub>, SiO<sub>2</sub>, and Si<sub>3</sub>N<sub>4</sub> was also studied for the reported etch

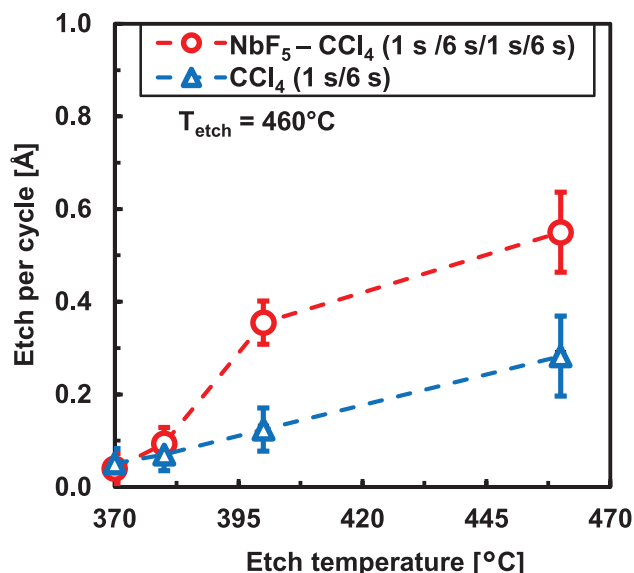


**Figure 3.** Effect of etch temperature on etch per cycle for the binary process (blue curve) as well as  $\text{CCl}_4$  alone (blue curve) process. Both the precursor pulses and the purge times were fixed to 1 and 6 s, respectively.

processes. **Figure 4** investigates the ability of the  $\text{CCl}_4$  alone CVE process to etch TiN selectively over  $\text{Al}_2\text{O}_3$ ,  $\text{SiO}_2$ , and  $\text{Si}_3\text{N}_4$  at 460 °C. The figure plots the etched thickness with the total number of etch cycles, where each cycle consisted of 1 s long  $\text{CCl}_4$  pulse followed by 6 s long  $\text{N}_2$  purge. EPC of 0.3 Å per cycle is deduced from a linear fit. After 500 etch cycles, about 13 nm TiN film is removed. No change in thickness is observed for  $\text{Al}_2\text{O}_3$ ,  $\text{SiO}_2$ , and  $\text{Si}_3\text{N}_4$  even after exposing them to 1000 cycles of 1 s long  $\text{CCl}_4$  pulses. Moreover, at temperatures below 460 °C,  $\text{CCl}_4$  is unable to etch  $\text{Al}_2\text{O}_3$ ,  $\text{SiO}_2$ , and  $\text{Si}_3\text{N}_4$  either and therefore the selective etching of TiN is possible within temperature window of 370–460 °C.

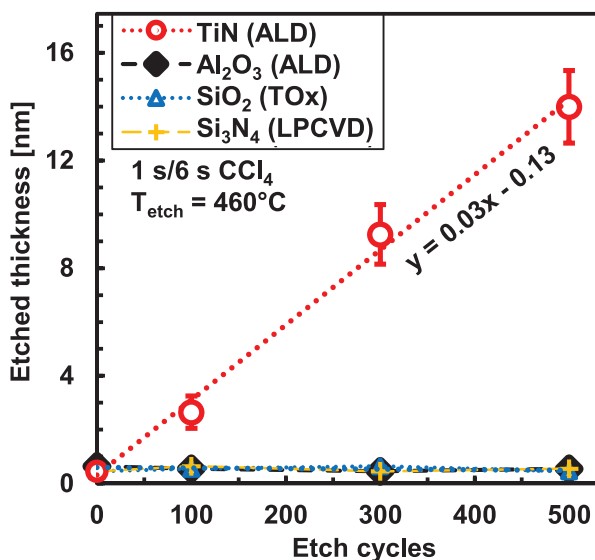


**Figure 4.** A change in the thickness values with total number of etch cycles at 460 °C for TiN,  $\text{SiO}_2$ ,  $\text{Al}_2\text{O}_3$ , and  $\text{Si}_3\text{N}_4$  films. A TiN is selectively etched away by  $\text{CCl}_4$  alone over other materials.

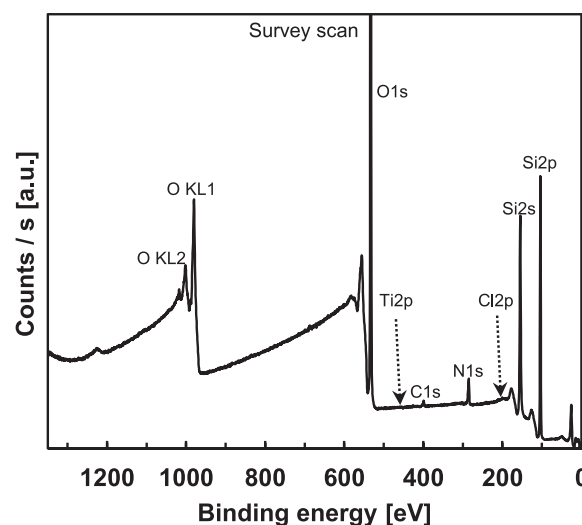


**Figure 5.** An X-ray photoelectron spectroscopy of  $\text{SiO}_2$  surface after complete removal of TiN film by  $\text{CCl}_4$  based CVE process at 460 °C.

#### 4.4. Post-Etch Analysis

After removing all 25 nm TiN film from the  $\text{SiO}_2$  substrate, an ex situ XPS spectra of the post-etch surface was measured and is shown in **Figure 5**. The main constituents of the remaining surface were 32.7 at% Si, 60.9 at% O, 5.1 at% C, and 1.2 at% of N, as revealed by XPS. Both the titanium and chlorine were below the detection limit of the XPS (<0.1 at%). The TiN film was etched at 460 °C by 600 CVE “cycles,” where each etch cycle was comprised of 3 s long  $\text{CCl}_4$  pulse followed by 6 s long  $\text{N}_2$  purge. After 600 etch cycles, about 30 nm TiN film was anticipated to have been etched. Keeping real etch applications in mind, this over-etch condition was deliberately chosen to remove any TiN remnants from the  $\text{SiO}_2$  surface. Moreover, it was important to study possible surface contamination arising from the etch process itself. The XPS analysis in **Figure 5** suggests that the surface is mostly composed of silicon, oxygen, and some adventitious carbon. In addition, about 1.2 at% nitrogen is seen. Titanium and chlorine were not detected. The detection limit of the particular XPS used here is 0.1 at%. The nitrogen and carbon signals were detected around 399.1 eV ( $\pm 0.1$  eV) and 284.8 eV ( $\pm 0.2$  eV), respectively, and are most probably due to organic surface contamination. Hence they can be associated with handling, storage and transportation of samples within non clean-room environment. The unetched silicon dioxide substrate shows no damage and matches with reference thermal  $\text{SiO}_2$  films.

The same sample from the **Figure 5** was subjected to a cross-sectional bright field transmission electron microscopy (BF-TEM). The BF-TEM images shown in **Figure 6** reveal that TiN was completely removed from the  $\text{SiO}_2$  surface by the  $\text{CCl}_4$ -only etch process. Spin-on carbon was deposited prior to the TEM imaging for highlighting the material contrast. The unetched sample is shown for reference and was not exactly the same sample. The TEM image depicts that after complete removal of the TiN film from the  $\text{SiO}_2$  surface, the surface appears to be clean and free of any surface contaminants from either the TiN film or the etch process.

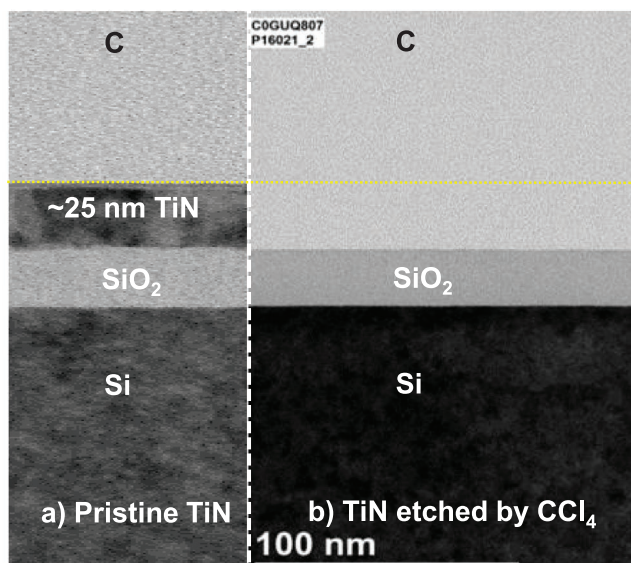


**Figure 6.** BF-TEM images of a) the reference unetched 25 nm TiN film on 22 nm SiO<sub>2</sub> film, b) after complete etching of 25 nm TiN film by 600 cycles of each 3 s long CCl<sub>4</sub> pulse separated by 6 s of N<sub>2</sub> purges.

**Figure 7** plots an XPS depth profile of the elements found in an about 9 nm TiN film remaining when the etch process was incomplete. The TiN film was etched by 300 cycles of the NbF<sub>5</sub>-CCl<sub>4</sub> etch process at 460 °C. The total of 60 s sputter time is estimated to etch about 1.8 nm of the TiN film. From the figure it can be seen that the surface contains about 26 at% carbon, 31 at% oxygen, 20 at% nitrogen, 15 at% titanium, and about 5 at% niobium. In addition, small amounts of silicon and fluorine were also detected with both being below 2 at%. The silicon signal is from the SiO<sub>2</sub> film underneath the TiN film. After 15 s of argon ion sputtering, the carbon signal is dropped to about 4 at% and goes further down to 3 at% after 1 min of sputtering. The atomic percentages for titanium,

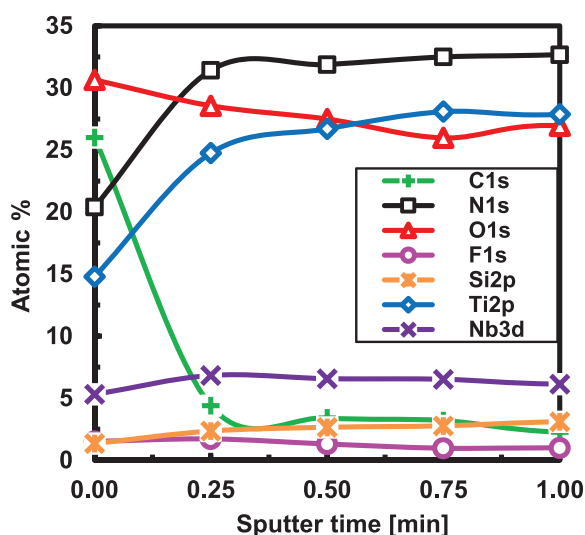


**Figure 7.** An XPS depth profiling through remaining TiN film after partial etching at 460 °C. Total 300 cycles were performed with 0.5 s of both NbF<sub>5</sub> and CCl<sub>4</sub> pulse lengths with 6 s of N<sub>2</sub> purges.

nitrogen, and oxygen are observed around 24, 32, and 28 respectively after sputtering the surface for 15 s. A fairly high niobium amount from 5 to 6 at% along with fluorine of about 0.9–1.7 at% may indicate that the NbF<sub>5</sub> is capable of either reacting or dissociating on TiN or the TiN surface modified by CCl<sub>4</sub>. The presence of niobium is evidently consistent with the DFT adsorption studies discussed in Section S1, Supporting Information. After sputtering for a minute, the presence of significant amounts of niobium, fluorine and carbon inside the top layer of the TiN films may be attributed to various reasons such as surface diffusion of the elements at etch temperatures preferentially through TiN grain boundaries, or increased surface area due to preferential etching along grain boundaries. They can also result from energetic argon ions bombarding the atoms deeper into the film. The absence of chlorine on or in the post-etch TiN layer points toward the formation of volatile products containing chlorine such as TiCl<sub>3</sub>, TiCl<sub>4</sub>, NbFCl<sub>3</sub>, NbClF<sub>4</sub>, and ClCN. All these compounds are predicted by the DFT simulation results.

**Figure 8** is a series of TEM images taken from 3D horizontal FIN structures. For a reference, schematic 1 provides an idea of such a 3D structure where the blue horizontal fins are SiO<sub>2</sub> fins and the black back-bone is silicon. This 3D structure was coated by a thin ALD TiN film<sup>[35]</sup> with extremely high conformality. One big advantage of gas-phase chemical etching over plasma-based etching is its capability to etch material from non-line-of-sight features of this sort. Another advantage can be maintaining conformality during the etching or thinning of the films. However, the non-self-limiting gas-phase chemical etching reactions can also affect the conformality. In order to improve the etch conformality, another etchant or control-reactant can be introduced to either improve conformality or modify the etch rate such that etching from non-line-of-sight features may follow more uniform removal.

In Figure 8a, a reference SiO<sub>2</sub> fin structure is covered by on average 3.3 nm pristine TiN film. The goal of this etching test was to observe the etch conformality and isotropic nature of the binary NbF<sub>5</sub>-CCl<sub>4</sub> etch process. The same sample was subjected to the binary etch process and from Figure 8b it can be concluded that after removal of about 0.8 nm of TiN conformally, no significant increase in the surface defects is observed. After applying over-etch the TiN is removed completely as seen in Figure 8c. From these TEM images, no etching of SiO<sub>2</sub> fins was observed, thus confirming the selectivity.

## 5. Summary

We successfully demonstrated two novel gas-phase etching processes for titanium nitride. The binary etching process is based on alternate exposures of NbF<sub>5</sub>-CCl<sub>4</sub>, each separated by N<sub>2</sub> purge. The chemical vapor etch (CVE) etch process utilizes CCl<sub>4</sub> exposures alone in a pulsed fashion. In addition, the selective etching of TiN with respect to SiO<sub>2</sub>, Si<sub>3</sub>N<sub>4</sub>, and Al<sub>2</sub>O<sub>3</sub> was also demonstrated. Furthermore, the gas-phase etching reported here also exhibits nondirectional etching from non-line-of-sight features.

From the first principles based DFT thermochemistry simulations the possible reactions and the candidate products



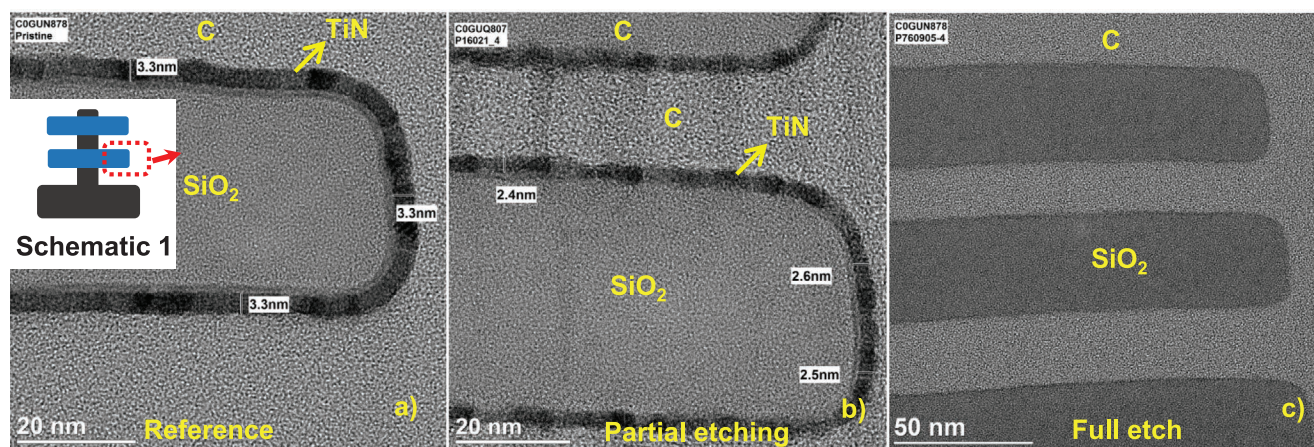


**Figure 8.** Cross-sectional bright field transmission electron micrograph (BF-TEM) of 3D structures: a) about 3.3 nm TiN film deposited on SiO<sub>2</sub> fins with lateral cavities, b) the same after about 0.8 nm TiN is etched by the NbF<sub>5</sub>-CCl<sub>4</sub> etch-process, and c) after removing the TiN film completely. The etching was performed at 460 °C.

involved in TiN etching were assessed. The surface etch mechanism is also presented in the Supporting Information.

In a two-step etch process, the DFT MD studies predict that the NbF<sub>5</sub> is able to fluorinate the TiN surface but is unable to etch it by itself. This non-etching is attributed to the formation NbNF<sub>x</sub> species that are difficult to desorb from the surface. In corroboration with this, the presence of Nb and F on surface was confirmed by XPS in Figure 7.

However, the simulations predict that in NbF<sub>5</sub>-CCl<sub>4</sub> etch process, NbF<sub>5</sub> could enhance the etch rate (favorable reaction free energy compared to CCl<sub>4</sub> only process) and this was experimentally verified. The Ti-F bonds are stronger and highly polar when compared to Ti-Cl bonds.<sup>[51]</sup> Thus, in comparison to Cl covered TiN surfaces, F covered TiN surfaces are more favorable for etching.

In the etching step, the CCl<sub>4</sub> has a tendency to chlorinate the Ti-F bonds and Nb atoms on the surface via halide-exchange mechanism<sup>[52]</sup> and hence fluorinated TiN and surface Nb as well as N atoms are etched by CCl<sub>4</sub> in the form of volatile compounds such as TiF<sub>4</sub>, NbFCl<sub>3</sub>, ClCN, and TiCl<sub>4</sub>.

For the NbF<sub>5</sub>-CCl<sub>4</sub> etch process, the EPC varied from 0.03 Å at 370 °C to a higher value of 0.55 Å at 460 °C. It was found that the EPC at 460 °C increases with an increase in either NbF<sub>5</sub> or CCl<sub>4</sub> pulse durations and a no clear self-limiting behavior is observed for either of the pulse durations.

Consistent with the simulation results, experiments found that CCl<sub>4</sub> is able to etch TiN spontaneously in a CVE fashion. The formation of volatile species such as TiCl<sub>3</sub> and ClCN is predicted by the thermochemical studies. The CCl<sub>4</sub>-only CVE process shows an EPC of about 0.07 Å per cycle at 370 °C, linearly increasing to about 0.3 Å per cycle at 460 °C. At 460 °C, for a given pulse duration, the TiN removal proceeds in a linear fashion with etch exposures.

After a complete removal of titanium nitride film by CCl<sub>4</sub>, the XPS as well as TEM analysis revealed a SiO<sub>2</sub> surface with no significant amounts of residues arising either from the etch process or the TiN film itself. In case of incomplete removal of TiN by the NbF<sub>5</sub>-CCl<sub>4</sub> process, XPS showed the presence of niobium and fluorine on the remaining TiN film. The absence of chlorine on the surface suggests effective formation

of volatile species containing chlorine, as predicted by the simulations. The TEM images verify uniform, conformal thinning, leading eventually to complete removal of TiN from 3D structures.

## Supporting Information

Supporting Information is available from the Wiley Online Library or from the author.

## Acknowledgements

The authors thank Eurofins EAG Materials Science, LLC (California, USA) for the TEM analysis. S.K.N. thanks ICHEC and the Science Foundation Ireland funded computing center of Tyndall National Institute for computer time. S.K.N. thanks Rita Mullins for help with reaction free energy calculations.

## Conflict of Interest

The authors declare no conflict of interest.

## Data Availability Statement

Research data are not shared.

## Keywords

atomic layer etching, density functional theory, thermal etching

Received: June 28, 2021

Revised: September 26, 2021

Published online: October 22, 2021

[1] A. Busnaina, *Nanomanufacturing Handbook*, 1 ed., CRC Press/Taylor & Francis, Boca Raton, FL 2007.

[2] J. Meena, S. Sze, U. Chand, T.-Y. Tseng, *Nanoscale Res. Lett.* **2014**, *9*, 526.



- [3] M. Ritala, J. Niinistö, *ECS Trans.* **2019**, 25, 641.
- [4] C. T. Carver, J. J. Plombon, P. E. Romero, S. Suri, T. A. Tronic, R. B. Turkot, *Solid State Sci. Technol.* **2015**, 4, N5005.
- [5] G. Oehrlein, D. Metzler, C. Li, *ECS J. Solid State Sci. Technol.* **2015**, 4, N5041.
- [6] K. J. Kanarik, T. Lill, E. A. Hudson, S. Sriraman, S. Tan, J. Marks, V. Vahedi, R. A. Gottscho, *J. Vac. Sci. Technol. A* **2015**, 33, 020802.
- [7] E. Marin, A. Lanzutti, F. Andreatta, M. Lekka, L. Guzman, L. Fedrizzi, *Corros. Rev.* **2011**, 29, 191.
- [8] V. Miikkulainen, M. Leskelä, M. Ritala, R. L. Puurunen, *J. Appl. Phys.* **2013**, 113, 021301.
- [9] P. O. Oviroh, R. Akbarzadeh, D. Pan, R. A. M. Coetzee, T.-C. Jen, *Sci. Technol. Adv. Mater.* **2019**, 20, 465.
- [10] S. M. George, *Acc. Chem. Res.* **2020**.
- [11] C. Fang, Y. Cao, D. Wu, A. Li, *Prog. Nat. Sci.* **2018**, 28, 667.
- [12] Y. Lee, S. M. George, *ACS Nano* **2015**, 9, 2061.
- [13] H. Dadgour, K. Endo, V. De, K. Banerjee, *IEEE Trans. Electron. Devices* **2010**, 57, 2504.
- [14] L. Lü, Wei-Feng; Dai, *Microelectron. J.* **2019**, 84, 54.
- [15] K. Matsuura, M. Hamada, T. Hamada, H. Tanigawa, T. Sakamoto, A. Hori, I. Muneta, T. Kawanago, K. Kakushima, K. Tsutsui, A. Ogura, H. Wakabayashi, *Jpn. J. Appl. Phys.* **2020**, 59, 080906.
- [16] H. Kim, *J. Vac. Sci. Technol. B Microelectron. and Nanometer Struct.* **2003**, 21, 2231.
- [17] M. Darnon, T. Chevolleau, D. Eon, L. Vallier, J. Torres, O. Joubert, *J. Vac. Sci. Technol. B: Microelectron. Nanometer Struct.–Process., Meas., Phenom.* **2006**, 24, 2262.
- [18] S. C. Abraham, *J. Vac. Sci. Technol. A Vac. Surf. Films* **1997**, 15, 702.
- [19] S. DeVries, E. A. De Silva, D. Canaperi, A. Simon, A. A. de la Pena, W. Wang, J. Maniscalco, L. Meli, B. Mendoza, in *31st Annual SEMI Advanced Semiconductor Manufacturing Conference (ASMC)*, IEEE, Piscataway, NJ **2020**, pp. 1–5.
- [20] S. L. Shinde, S. Ishii, T. Nagao, *ACS Appl. Mater. Interfaces* **2019**, 11, 21965.
- [21] J. Goscinia, F. B. Atar, B. Corbett, M. Rasras, *ACS Omega* **2019**.
- [22] F. Mehmood, R. Pachter, N. R. Murphy, W. E. Johnson, *J. Appl. Phys.* **2015**, 118, 195302.
- [23] P. Patsalas, N. Kalfagiannis, S. Kassavetis, *Materials* **2015**, 8, 3128.
- [24] E. I. Cooper, R. Rajaram, M. Payne, S. Lippy, *Solid State Phenom.* **2012**, 195, 143.
- [25] Y. Liu, T. Kamei, K. Endo, S. O'uchi, J. Tsukada, H. Yamauchi, T. Hayashida, Y. Ishikawa, T. Matsukawa, K. Sakamoto, A. Ogura, M. Masahara, *Jpn. J. Appl. Phys.* **2010**, 49, 06GH18.
- [26] D. Bhattacharyya, S. Kuchibhatla, A. Sehgal, Y. P. Shen, W. Haiting, J. Prasad, in *26th Annual SEMI Advanced Semiconductor Manufacturing Conference (ASMC)*, IEEE, Piscataway, NJ **2015**, pp. 305–308.
- [27] J. Tonotani, T. Iwamoto, F. Sato, K. Hattori, S. Ohmi, H. Iwai, *J. Vac. Sci. Technol., B: Microelectron. Nanometer Struct.–Process., Meas., Phenom.* **2003**, 21, 2163.
- [28] Y.-Y. Wang, Y.-H. Joo, C.-I. Kim, *J. Nanosci. Nanotechnol.* **2016**, 16, 12933.
- [29] N. Marchack, J. M. Papalia, S. Engelmann, E. A. Joseph, *J. Vac. Sci. Technol. Vac. Surf. Films* **2017**, 35, 05C314.
- [30] K. Shinoda, N. Miyoshi, H. Kobayashi, M. Izawa, K. Ishikawa, M. Hori, *J. Phys. D: Appl. Phys.* **2019**, 52, 475106.
- [31] Y. Lee, S. M. George, *Chem. Mater.* **2017**, 29, 8202.
- [32] V. Sharma, T. Blomberg, S. Haukka, S. Cembella, M. E. Givens, M. Tuominen, R. Odedra, W. Graff, M. Ritala, *Appl. Surf. Sci.* **2020**, 52, 148309.
- [33] G. Dingemans, C. Van Helvoirt, M. Van de Sanden, W. M. Kessels, in *ECS Transactions [ECS 219th ECS Meeting - Montreal, QC, Canada (May 1 - May 6, 2011)] - Plasma-Assisted Atomic Layer Deposition of Low Temperature SiO<sub>2</sub>*, IOP Publishing, Bristol **2011**, pp. 191–204.
- [34] L. Gosset, J.-F. Damlencourt, O. Renault, D. Rouchon, P. Holliger, A. Ermolieff, I. Trimaille, J.-J. Ganem, F. Martin, M.-N. Séméria, *J. Non-Cryst. Solids* **2002**, 303, 17.
- [35] C. H. Ahn, S. G. Cho, H. J. Lee, K. H. Park, S. H. Jeong, *Metals Mater. Int.* **2001**, 7, 621.
- [36] J. V. Michael, K. P. Lim, S. S. Kumaran, J. H. Kiefer, *J. Phys. Chem.* **1993**, 97, 1914.
- [37] F. Huang, H. Zhao, A. Yan, Z. Li, H. Liang, Q. Gao, Y. Qiang, *J. Alloys Compd.* **2017**, 695, 489.
- [38] R. J. M. Konings, *Struct. Chem.* **1994**, 5, 9.
- [39] V. Sharma, S. D. Elliott, T. Blomberg, S. Haukka, M. E. Givens, M. Tuominen, M. Ritala, *Chem. Mater.* **2021**, 33, 2883.
- [40] G. Kresse, J. Furthmüller, *Phys. Rev. B* **1996**, 54, 11169.
- [41] G. Kresse, D. Joubert, *Phys. Rev. B* **1999**, 59, 1758.
- [42] J. P. Perdew, K. Burke, M. Ernzerhof, *Phys. Rev. Lett.* **1996**, 77, 3865.
- [43] P. Blochl, *Phys. Rev. B* **1994**, 50, 17953.
- [44] TURBOMOLE V6.2 2010, a development of University of Karlsruhe and Forschungszentrum Karlsruhe GmbH, 1989–2007, TURBOMOLE GmbH (2010), <http://www.turbomole.com> (accessed: November 2019).
- [45] A. Togo, I. Tanaka, *Scr. Mater.* **2015**, 108, 1.
- [46] G. Ramanath, J. E. Greene, J. R. A. Carlsson, L. H. Allen, V. C. Hornback, D. J. Allman, *J. Appl. Phys.* **1999**, 85, 1961.
- [47] H. Sekimoto, Y. Nose, T. Uda, H. Sugimura, *High Temp. Mater. Processes* **2011**, 30, 435.
- [48] K. Kelley, A. Mah, *Metallurgical Thermochemistry of Titanium*, Report of investigations/U.S. Dept. of the Interior, Bureau of Mines, University of Michigan, Ann Arbor, MI **1959**.
- [49] F. P. Pike, C. T. Foster, *J. Chem. Eng. Data* **1959**, 4, 305.
- [50] E. H. Hall, J. M. Blocher, I. E. Campbell, *J. Electrochem. Soc.* **1958**, 105, 275.
- [51] S. P. Webb, M. S. Gordon, *J. Am. Chem. Soc.* **1999**, 121, 2552.
- [52] G. Evano, A. Nitelet, P. Thilmany, D. F. Dewez, *Front. Chem.* **2018**, 6, 114.